

ZERO-ORDER SHARPNESS-AWARE MINIMIZATION

Yao Fu

Xi'an Jiaotong University
SGIT AI Lab, State Grid Corporation of China
fyao56@stu.xjtu.edu.cn

Yihang Jin

Xi'an Jiaotong University
yihangjin@stu.xjtu.edu.cn

Chunxia Zhang

Xi'an Jiaotong University
cxzhang@mail.xjtu.edu.cn

Junmin Liu

Xi'an Jiaotong University
junminliu@mail.xjtu.edu.cn

Haishan Ye*

SGIT AI Lab, State Grid Corporation of China
hsye_cs@outlook.com

ABSTRACT

Prompt learning has become a key method for adapting large language models to specific tasks with limited data. However, traditional gradient-based optimization methods for tuning prompts are computationally intensive, posing challenges for efficiency. We introduce ZOSA (Zero-Order Sharpness-Aware Minimization), a novel optimization framework that integrates zero-order optimization with sharpness-aware minimization to enhance prompt tuning. ZOSA employs Rademacher perturbation vectors to estimate gradients without requiring back-propagation. By incorporating sharpness-aware principles, it targets flat minima in the loss landscape, improving generalization. An adaptive learning rate, guided by loss variability, further ensures stable convergence. Experiments on few-shot learning tasks, such as text classification and natural language inference, show that ZOSA significantly outperforms existing methods. With its theoretical foundation and computational efficiency, ZOSA offers a practical solution for prompt-based learning in resource-limited settings.

1 INTRODUCTION

Zeroth-order (ZO) optimization has become indispensable in machine learning scenarios where gradient information is inaccessible or computationally prohibitive, such as black-box adversarial attacks (Ru et al., 2020; Hiranandani et al., 2021) and memory-constrained fine-tuning of large language models (LLMs) (Malladi et al., 2023a; Zhang et al., 2024b). Unlike first-order methods that rely on backpropagation, ZO algorithms estimate gradients solely through function evaluations, enabling applications in resource-limited environments (Liu et al., 2018b; Chen et al., 2019; Shu et al., 2024).

However, traditional ZO methods suffer from high variance in gradient estimates, leading to slow convergence and suboptimal generalization, particularly in high-dimensional non-convex landscapes (Chen et al., 2019; Nazari et al., 2020). Adaptive ZO optimizers, such as ZO-AdaMM (Chen et al., 2019; Nazari et al., 2020), attempt to mitigate these issues by incorporating moment estimates for better scaling of updates. Yet, they underutilize historical information, resulting in noisy estimates and limited performance gains (Shu et al., 2025). Recent advances like R-AdaZO (Shu et al., 2025) refine moment utilization through variance reduction on first-moment estimates and improved second-moment approximations, achieving faster convergence. Meanwhile, sharpness-aware minimization (SAM) (Foret et al., 2021) has emerged as a powerful technique in first-order settings to enhance generalization by seeking flat minima, but its direct application to ZO is challenging due to the absence of gradients. SABO (Ye et al., 2024) extends SAM to zero-order optimization by reparameterizing objectives over Gaussian distributions and approximating sharpness-aware updates via

stochastic gradients. Similarly, FZOO (Dang & Others, 2025) accelerates ZO fine-tuning of LLMs using batched one-sided estimates and adaptive step-sizes based on loss standard deviations, approaching Adam-like speeds with inference-level memory.

Despite these progresses, existing ZO methods often trade off between memory efficiency, convergence speed, and generalization. For instance, MeZO (Malladi et al., 2023b) reduces memory to inference levels but requires significantly more forward passes than Adam. To bridge this gap, we introduce Zeroth-Order Sharpness-Aware (ZOSA) optimization, a novel adaptive ZO optimizer that integrates sharpness-aware mechanisms with refined variance reduction and adaptive scaling. ZOSA employs batched Rademacher perturbations for efficient one-sided gradient estimates, computes adaptive step-sizes using the standard deviation of batch losses, and incorporates a SAM-like perturbation at a scaled point to promote flat minima and better generalization. This design reduces variance in estimates (building on R-AdaZO (Shu et al., 2025)) while minimizing forward passes. Our contributions are summarized as follows:

- We propose ZOSA, an efficient zeroth-order (ZO) optimizer that seamlessly combines sharpness-aware updates with adaptive loss-variance-based scaling, with minimal inference-time memory overhead. The algorithm features a simple design, requiring no additional updates to a Σ matrix (thus avoiding the extra storage burden and computational complexity associated with Σ matrix updates), it offers fast computation, significantly fewer function queries, and accuracy superior to or on par with SABO, which is the state-of-the-art of shape-aware ZO algorithm, providing a practical and easy-to-implement solution for ZO optimization.
- We provide comprehensive theoretical analysis, including proofs of equivalence to a SAM rule, rigorous variance reduction bounds, and convergence guarantees under standard assumptions, further solidifying its theoretical foundations.
- Extensive experiments on synthetic problems and large language model (LLM) fine-tuning tasks demonstrate ZOSA’s superiority in convergence speed, resource efficiency, and performance stability, highlighting its potential in real-world applications.

2 RELATED WORKS

ZO optimization research primarily advances in gradient estimation and update rules, with growing emphasis on adaptivity, generalization, and applications to large-scale models like LLMs. Early ZO methods rely on finite-difference approximations for gradients, such as two-point estimates (Liu et al., 2018b;a). To address high-dimensional challenges, random direction sampling (e.g., Gaussian, Rademacher, or coordinate-wise) reduces query complexity while maintaining unbiased estimates (Chen et al., 2019; Shu et al., 2024; Nesterov & Spokoiny, 2011). Recent works like MeZO (Malladi et al., 2023b) apply these techniques to LLM fine-tuning, replacing backpropagation with forward passes to achieve inference-level memory usage. However, MeZO’s fixed step-sizes lead to slow convergence, often requiring 10-20 \times more iterations than first-order methods, as practitioners highlight its dependence on local Hessian rank rather than parameter count.

ZO for LLM Fine-Tuning. With the rise of LLMs, ZO has been tailored for memory-efficient fine-tuning in resource-constrained settings. For instance, DP-ZO (Lin et al., 2024) introduces differential privacy into ZO for private LLM adaptation using forward-only perturbations. Quantized variants like QuZO (Qu et al., 2025) enable low-bit ZO fine-tuning, achieving performance comparable to MeZO on tasks like GLUE while reducing computational overhead. HiZOO (Cai et al., 2024) leverages diagonal Hessian approximations to enhance ZO updates, and FedMeZO (Zhang et al., 2024a) extends this to federated learning, proving convergence in distributed settings. SubZero (Chen et al., 2024a) tackles sparsity by optimizing in random subspaces, mitigating dimensionality curses in billion-parameter models. These methods collectively demonstrate ZO’s potential for LLM adaptation but often overlook generalization in non-convex landscapes (Zhang et al., 2024b; Malladi et al., 2023b).

Adaptive ZO Optimizers and Variance Reduction. Adaptive methods improve upon basic SGD-like ZO by incorporating momentum and scaling. ZO-AdaMM (Chen et al., 2019; Nazari et al., 2020) adapts Adam’s moments to ZO but suffers from high-variance estimates in noisy environments. R-AdaZO (Shu et al., 2025) overcomes this by providing the first analysis of variance reduction via first-moment estimates and refining second moments for better geometry capture, yielding faster convergence than ZO-AdaMM. FZOO (Dang & Others, 2025) accelerates ZO through batched

Rademacher perturbations and adaptive step-sizes based on batch loss standard deviations, emulating normalized-SGD (You et al., 2019) without momentum costs, and seamlessly integrates with PEFT techniques like LoRA (Hu et al., 2021) for further memory savings. Additional variance reduction approaches, such as LOZO (Chen et al., 2024b), use low-rank gradient estimators to capture low-dimensional structures in LLM loss landscapes (Zhou et al., 2025).

Sharpness-Aware and Zero-Order Optimization. Sharpness-aware minimization (SAM) (Foret et al., 2021) promotes generalization in first-order optimization by seeking flat minima through neighborhood maximization, but it requires gradients. Extensions like VS-SAM (Liu et al., 2023) suppress variance in perturbations for stable training. In zero-order settings, SABO (Ye et al., 2024) reparameterizes objectives over Gaussian distributions to approximate sharpness-aware stochastic gradients, with proven convergence and generalization bounds. SharpZO (Yang et al., 2025) hybridizes this for vision-language models, enhancing ZO prompt optimization. These align with empirical findings that flat minima correlate with better performance (Dziugaite & Roy, 2017; Petzka & Sminchisescu, 2021; Andriushchenko & Flammarion, 2022). In LLM contexts, sharpness-aware ZO could alleviate overfitting in zero-order tuning (Sun et al., 2022b; 2023), though existing methods like SAM variants (Huang et al., 2024) are limited to gradient-based scenarios.

ZOSA builds on these foundations by fusing variance-reduced adaptive scaling (Shu et al., 2025), efficient batched estimation, and sharpness-aware updates (Ye et al., 2024), while incorporating elements from recent LLM-specific ZO works (Lin et al., 2024; Cai et al., 2024), to provide a unified, memory-efficient framework for generalizable optimization.

3 METHODOLOGY

In the following, we first briefly review the preliminaries of classical zeroth-order gradient estimation (Section 3.1). We then present the motivation and complete workflow of our ZOSA optimizer (Section 3.2), and finally offer a theoretical analysis of the gradient estimation properties (Section 3.3).

3.1 PRELIMINARIES

Consider a labeled dataset $\mathcal{D} = \{(x_i, y_i)\}_{i=1}^{|\mathcal{D}|}$, where a mini-batch $\mathcal{B} \subset \mathcal{D}$ has size $|\mathcal{B}|$. Let $\theta \in \mathbb{R}^d$ denote all trainable parameters of the LLM, and let $L(\theta; \mathcal{B})$ be the empirical loss on \mathcal{B} .

Classical ZO Gradient Estimation Given a perturbation radius $\epsilon > 0$ and $z \in \mathbb{R}^d$ sampled as $z \sim \mathcal{N}(0, I_d)$, the Classical ZO estimates the gradient on \mathcal{B} via:

$$\hat{\nabla} L(\theta; \mathcal{B}) = \frac{L(\theta + \epsilon z; \mathcal{B}) - L(\theta - \epsilon z; \mathcal{B})}{2\epsilon} z \approx zz^\top \nabla L(\theta; \mathcal{B}). \quad (1)$$

Averaging over N i.i.d. draws $\{z_i\}_{i=1}^N$ yields the n -ZO estimator $\hat{\nabla}_N L = \frac{1}{N} \sum_{i=1}^N \hat{\nabla}_i L$.

From classical ZO to ZO-SGD. Replacing the back-propagation gradient in SGD with the classical ZO estimate gives the zeroth-order update $\theta_{t+1} = \theta_t - \eta_t \hat{\nabla} L(\theta_t; \mathcal{B}_t)$. MeZO realizes this update in-place with the memory tricks above and serves as a baseline for improvements. The introduction of Fast Zeroth-Order Optimizer (FZOO) is in Appendix A.1.

3.2 MOTIVATION OF ZOSA

To enhance generalization while maintaining efficiency, ZOSA builds upon FZOO by incorporating sharpness-aware minimization (SAM) principles. This integration targets flatter minima in the loss landscape. Specifically, ZOSA first estimates the gradient at the current parameters using batched Rademacher perturbations, computes an adaptive perturbation based on the estimated gradient normalized by loss variance, and then performs a second gradient estimation at the perturbed point for the final update. This dual-estimation approach combines FZOO’s memory-efficient zeroth-order strategy with SAM-like sharpness awareness, normalized via variance for stability in high-dimensional spaces.

Letting u_1, \dots, u_m be m i.i.d. Rademacher random vectors in \mathbb{R}^d , we construct the initial gradient estimation at the original point θ_t by function value queries $l_i = L(\theta_t + \epsilon u_i; \mathcal{B}_t)$, and $l_0 = L(\theta_t; \mathcal{B}_t)$.

Algorithm 1 ZOSA (Zero-Order Sharpness-Aware) Optimizer

Require: Model parameters θ , loss function $L(\theta)$, sharpness-aware radius ρ , perturbation scale ϵ , number of sampled directions m , learning rate η

Ensure: Optimized model parameters θ

```
1: Initialize  $\theta$ 
2: while not converged do
3:   Estimate gradient at the original point:
4:   Generate  $m$  Rademacher perturbation vectors  $u_i$  for  $i = 1$  to  $m$ 
5:   Compute original loss  $l_0 = L(\theta)$ 
6:   for each  $u_i$  do
7:     Perturb parameters:  $\theta' = \theta + \epsilon \cdot u_i$ 
8:     Compute perturbed loss  $l_i = L(\theta')$ 
9:     Restore parameters:  $\theta' = \theta$ 
10:  end for
11:  Estimate gradient  $g_t = \frac{1}{m} \sum_{i=1}^m \frac{l_i - l_0}{\epsilon} \cdot u_i$ 
12:  Compute standard deviation for adaptive step size:
13:   $\sigma_t = \text{std}([l_i \text{ for } i \text{ in } 1 \text{ to } m])$ 
14:  Sharpness-aware perturbation:
15:  if  $\sigma_t > 0$  then
16:    Compute perturbation  $\epsilon_{\text{sam}} = \rho \cdot \frac{g_t}{\sigma_t}$ 
17:  else
18:     $\epsilon_{\text{sam}} = 0$ 
19:  end if
20:  Estimate gradient at the perturbed point:
21:  Perturb parameters:  $\theta_{\text{pert}} = \theta + \epsilon_{\text{sam}}$ 
22:  Generate  $m$  new Rademacher perturbation vectors  $u_{\text{pert},i}$  for  $i = 1$  to  $m$ 
23:  Compute perturbed point loss  $l_{\text{pert}} = L(\theta_{\text{pert}})$ 
24:  for each  $u_{\text{pert},i}$  do
25:    Perturb parameters:  $\theta'_{\text{pert}} = \theta_{\text{pert}} + \epsilon \cdot u_{\text{pert},i}$ 
26:    Compute perturbed loss  $l_{i,\text{pert}} = L(\theta'_{\text{pert}})$ 
27:    Restore parameters:  $\theta'_{\text{pert}} = \theta_{\text{pert}}$ 
28:  end for
29:  Estimate gradient  $g_{\text{pert}} = \frac{1}{m} \sum_{i=1}^m \frac{l_{i,\text{pert}} - l_{\text{pert}}}{\epsilon} \cdot u_{\text{pert},i}$ 
30:  Compute adaptive learning rate at perturbed point:
31:   $\sigma_{t,\text{pert}} = \text{std}([l_{i,\text{pert}} \text{ for } i \text{ in } 1 \text{ to } m])$ 
32:  Set adaptive learning rate  $\eta_{\text{adaptive}} = \begin{cases} \frac{\eta}{\sigma_{t,\text{pert}}} & \text{if } \sigma_{t,\text{pert}} > 0 \\ \eta & \text{otherwise} \end{cases}$ 
33:  Restore original parameters:
34:   $\theta_{\text{pert}} = \theta$ 
35:  Update parameters:
36:   $\theta = \theta - \eta_{\text{adaptive}} \cdot g_{\text{pert}}$ 
37: end while
38: return  $\theta$ 
```

That is, the gradient estimate g_t is computed by averaging m one-sided difference estimates

$$g_t = \frac{1}{\epsilon m} \sum_{i=1}^m (l_i - l_0) u_i. \quad (2)$$

The estimated variance σ_t^2 at the original point is computed as:

$$\sigma_t^2 = \frac{1}{m-1} \sum_{i=1}^m \left(l_i - \frac{1}{m} \sum_{j=1}^m l_j \right)^2. \quad (3)$$

Next, the sharpness-aware perturbation is calculated as $\epsilon_{\text{sam}} = \rho \frac{g_t}{\sigma_t}$ (if $\sigma_t > 0$, else zero), where ρ is the SAM perturbation radius. We then move to the perturbed point $\theta_t + \epsilon_{\text{sam}}$ and generate a new set

of m i.i.d. Rademacher vectors $u_{\text{pert},1}, \dots, u_{\text{pert},m}$. Compute $l_{\text{pert},i} = L(\theta_t + \epsilon_{\text{sam}} + \epsilon u_{\text{pert},i}; \mathcal{B}_t)$ and $l_{\text{pert}} = L(\theta_t + \epsilon_{\text{sam}}; \mathcal{B}_t)$. The gradient estimate at the perturbed point g_{pert} is:

$$g_{\text{pert}} = \frac{1}{\epsilon m} \sum_{i=1}^m (l_{\text{pert},i} - l_{\text{pert}}) u_{\text{pert},i}. \quad (4)$$

The estimated variance at the perturbed point $\sigma_{t,\text{pert}}^2$ is:

$$\sigma_{t,\text{pert}}^2 = \frac{1}{m-1} \sum_{i=1}^m \left(l_{\text{pert},i} - \frac{1}{m} \sum_{j=1}^m l_{\text{pert},j} \right)^2. \quad (5)$$

Our ZOSA updates the parameters (after restoring to the original θ_t) according to:

$$\theta_{t+1} = \theta_t - \eta_t \frac{g_{\text{pert}}}{\sigma_{t,\text{pert}}}, \quad (6)$$

where η_t is the base learning rate. The detailed implementation of ZOSA is outlined in Alg. 1.

3.3 UNDERSTANDING ZOSA’S GRADIENT ESTIMATION

Property 3.1 (Dang & Others, 2025) For the zeroth-order gradient estimator $\hat{g} = \frac{1}{m} \sum_{i=1}^m \hat{g}_i$, where $\hat{g}_i = \frac{L(\theta + \epsilon u_i) - L(\theta)}{\epsilon} u_i$ and u_i are i.i.d. Rademacher vectors in \mathbb{R}^d , under the assumption that $L(\theta)$ is twice continuously differentiable with \mathcal{L} -Lipschitz gradients, the expected mean squared error satisfies:

$$\mathbb{E}[\|\hat{g} - \nabla L(\theta)\|^2] \leq \frac{\sigma^2}{m} + O(\epsilon), \quad (7)$$

where $\sigma^2 = (d-1)\|\nabla L(\theta)\|^2 + O(\epsilon)$ bounds the variance of the loss differences, ϵ is the perturbation scale, and m is the number of sampled directions. The proof is provided in Appendix A.2.

Using Rademacher vectors instead of Gaussian perturbations offers computational advantages, as perturbations involve only sign flips, enabling efficient batched forward passes via CUDA parallelism. This fuses multiple matrix multiplications into a single kernel, reducing wall-time by a factor proportional to m , making ZOSA suitable for high-dimensional LLM fine-tuning.

Property 3.2 (Dang & Others, 2025) ZOSA employs an adaptive learning rate $\eta/\sigma_{t,\text{pert}}$, where $\sigma_{t,\text{pert}}$ is the standard deviation of the perturbed losses at the perturbed point. This design draws inspiration from normalized-SGD principles, adapting step sizes based on local curvature without the overhead of momentum. The variance of the loss perturbations satisfies:

$$\mathbb{E}[\sigma_t^2] = \epsilon^2 \|\nabla L(\theta_t)\|^2 + O(\epsilon^3), \quad (8)$$

implying $\sigma_t \approx \epsilon \|\nabla L(\theta_t)\|$. Thus, dividing by σ_t normalizes the gradient estimate, yielding updates akin to:

$$\theta_{t+1} = \theta_t - \frac{\eta}{\sigma_{t,\text{pert}}} g_{\text{pert}} \approx \theta_t - \eta \frac{\nabla L(\theta_t + \epsilon_{\text{sam}})}{\|\nabla L(\theta_t + \epsilon_{\text{sam}})\|}. \quad (9)$$

This receives larger steps in flat regions (small σ_t) and smaller steps in steep regions, mirroring Adam-style adaptivity at inference-level memory cost. It establishes ZOSA’s equivalence to normalized-SAM in the zeroth-order domain, enhancing convergence speed and stability. The proof and Equivalence to SAM is provided in Appendix A.3.

4 ANALYSIS

4.1 CONVERGENCE ANALYSIS OF ZOSA

This section derives the convergence properties of ZOSA, showing that the average squared gradient norm decreases over iterations under certain assumptions.

Assumption 4.1 (Smoothness). Suppose that the loss function $L(\theta)$ is \mathcal{L} -smooth, i.e., for all $\theta_1, \theta_2 \in \mathbb{R}^d$, it holds that:

$$L(\theta_2) \leq L(\theta_1) + \langle \nabla L(\theta_1), \theta_2 - \theta_1 \rangle + \frac{\mathcal{L}}{2} \|\theta_2 - \theta_1\|^2. \quad (10)$$

Assumption 4.2 (Bounded Variance). The stochastic gradient $\nabla L(\theta, \mathcal{B})$ has bounded variance:

$$\mathbb{E} \|\nabla L(\theta, \mathcal{B})\|^2 \leq \|\nabla L(\theta)\|^2 + \mathcal{V}^2, \quad (11)$$

where \mathcal{V}^2 is a constant. The above is a standard assumption for stochastic gradient descent.

$$\mathbb{E} \|\hat{g}_t\|^2 = \frac{N+d-1}{N} \|\nabla L(\theta_t)\|^2 + \gamma_t, \quad \gamma_t = O(\epsilon), \quad (12)$$

$$\mathbb{E} \sigma_t^2 = \epsilon^2 \|\nabla L(\theta_t)\|^2 + \zeta_t, \quad \zeta_t = O(\epsilon^3). \quad (13)$$

This implies that $\sigma_t \approx \epsilon \|\nabla L(\theta_t)\|$, and the effective perturbation magnitude in ZOSA is approximately ρ after normalization (i.e., the division by σ_t effectively scales to match the unit gradient direction with radius ρ).

Theorem 4.3 (Convergence of ZOSA). Assume the objective function $L(\theta)$ is \mathcal{L} -smooth and non-convex with a lower bound L^* , and the loss perturbations satisfy bounded variance ($\mathbb{E}[(l_i - L(\theta))^2] \leq \sigma^2$). The update rule is $\theta_{t+1} = \theta_t - \frac{\eta}{\sigma_{t,\text{pert}}} g_{\text{pert}}$, where g_{pert} is the zeroth-order gradient estimate at the perturbed point $\theta_t + \epsilon_{\text{sam}}$, with $\epsilon_{\text{sam}} = \rho \frac{g_t}{\sigma_t}$ ($\rho > 0$ is the sharpness radius), m is the number of queries per estimate (Rademacher perturbations), and ϵ is the perturbation scale. Choose $\eta_t \leq \frac{m}{16d\mathcal{L}}$, $\epsilon \leq \frac{1}{\sqrt{d\mathcal{L}}}$, and $\rho \leq \frac{1}{4\mathcal{L}}$. Then, after T iterations, ZOSA satisfies:

$$\frac{1}{T} \sum_{t=1}^T \mathbb{E} \|\nabla L(\theta_t)\|^2 \leq \frac{2(L(\theta_1) - L^*)}{\eta T} + 2\rho\mathcal{L} + \sqrt{\frac{4d\mathcal{L}(L(\theta_1) - L^*)(\sigma^2 + \epsilon^2 G^2)}{m\eta T}} + O(\epsilon^2 d\mathcal{L}), \quad (14)$$

Additionally, the algorithm biases towards approximately flat minima: for the output $\bar{\theta}$ (randomly selected from $\{\theta_t\}$), $\mathbb{E}[\text{Tr}(\nabla^2 L(\bar{\theta}))] \leq \min_{\theta^* \in \Theta^*} \text{Tr}(\nabla^2 L(\theta^*)) + O(\rho + \epsilon\sqrt{d})$, where Θ^* is the set of minimizers and Tr denotes the trace of the Hessian (measuring flatness).

Remarks: ZOSA introduces the $\rho\mathcal{L}$ term for sharpness control and an explicit bias towards low-trace Hessians, enhancing generalization. The rate is $O(1/\sqrt{T})$ similar to standard ZO-SGD, but the variance term $\sqrt{d/mT}$ reflects query efficiency, with ρ and ϵ terms arising from the SAM bias and perturbation scale. The proof is provided in Appendix B.1.

4.2 GENERALIZATION ERROR ANALYSIS FOR ZOSA

In this section, we derive a generalization error bound for the ZOSA optimizer. The goal is to quantify how well the ZOSA optimizer generalizes from training data to unseen data by bounding the expected loss over a distribution of parameters, leveraging a PAC-Bayesian framework.

4.2.1 PROBLEM SETUP AND NOTATION

Consider a training dataset $\mathcal{S} = \{(X_i, y_i)\}_{i=1}^M$ with M i.i.d. samples drawn from a true data distribution $P(X, y)$. The empirical loss over \mathcal{S} is defined as:

$$F(\theta; \mathcal{S}) = \frac{1}{M} \sum_{i=1}^M l(\theta; (X_i, y_i)), \quad (15)$$

where $l(\theta; (X, y))$ is the loss function (e.g., cross-entropy loss) evaluated at parameter θ . The population loss over the true distribution is:

$$\mathbb{E}_{P(X, y)}[F(\theta; (X, y))] = \mathbb{E}_{P(X, y)}[l(\theta; (X, y))]. \quad (16)$$

For ZOSA, the parameters are point estimates $\theta_t \in \mathbb{R}^d$ at iteration t , and $\sigma_t > 0$ is the adaptive standard deviation of perturbed losses computed at the current point. The objective function is the empirical loss:

$$J(\theta_t) = F(\theta_t; \mathcal{S}). \quad (17)$$

To enhance generalization, ZOSA adopts a sharpness-aware minimization strategy, seeking flat minima in the parameter space. We define a neighborhood around θ_t using the L_2 norm with an adaptive radius:

$$\mathcal{C}(\theta_t) = \{\delta \in \mathbb{R}^d \mid \|\delta\|_2 \leq \rho/\sigma_t\}, \quad (18)$$

where $\rho > 0$ controls the base neighborhood size, and the radius is adaptively scaled by σ_t to account for local loss variability. The sharpness-aware objective for ZOSA is:

$$\min_{\theta_t} \max_{\delta \in \mathcal{C}(\theta_t)} J(\theta_t + \delta), \quad (19)$$

where $J(\theta_t + \delta) = F(\theta_t + \delta; \mathcal{S})$. This formulation ensures robustness by minimizing the worst-case loss within the adaptive neighborhood.

Theorem 4.4 (Generalization Bound for ZOSA). Let the loss function $F(\theta; (X, y))$ be convex with respect to θ . For any $\theta_t \in \mathbb{R}^d$ and $\sigma_t > 0$, with probability at least $1 - \kappa$ over the draw of the training set \mathcal{S} with M i.i.d. samples from $P(X, y)$:

$$\mathbb{E}_{P(X, y)}[F(\theta_t; (X, y))] \leq \max_{\|\delta\|_2 \leq \rho/\sigma_t} F(\theta_t + \delta; \mathcal{S}) \quad (20)$$

$$+ \sqrt{\frac{k \log \left(1 + \frac{\|\theta_t\|_2^2}{(\rho/\sigma_t)^2 \left(1 + \sqrt{\frac{\log M}{k}} \right)^2} \right) + 4 \log \frac{M}{\kappa} + \tilde{O}(1)}{M - 1}}, \quad (21)$$

where $k = d$ is the number of parameters, σ_t is the adaptive standard deviation of the perturbed losses at iteration t (as computed in ZOSA), and the neighborhood radius is adaptively scaled by σ_t . This bound links the generalization error of the parameter θ_t to the sharpness-aware objective and a complexity term dependent on the adaptive neighborhood size ρ/σ_t , dataset size M , parameter dimension k , and confidence parameter κ . The proof is provided in Appendix B.2.

5 EXPERIMENTS

5.1 SYNTHETIC FUNCTIONS

To assess the convergence of ZOSA in high-dimensional settings, we evaluated its performance on four widely used synthetic functions, including quadratic, cubic, Levy, and Rosenbrock functions (detailed definitions provided in Appendix C.1). These functions serve as standard benchmarks for optimization algorithms, enabling us to examine ZOSA’s handling of smooth, convex landscapes and challenging, ill-conditioned non-convex surfaces, where variance in zeroth-order estimates plays a critical role.

We conduct experiments in a high-dimensional regime with $d = 10,000$, running for $T = 40,000$ iterations. The smoothing parameter μ is set to 5^{-3} , and the number of queries per iteration $K = 1000$. For ZOSA, we use $\rho = 1e - 5$, $\epsilon = 10^{-3}$, and $m = 1000$ Rademacher vectors, tuned via grid search on a validation set. We compare ZOSA against established adaptive ZO baselines: ZO-signSGD, ZO-AdaMM, and ZO-RMSProp. All baselines share the same query budget and are initialized at θ_0 drawn from $\mathcal{N}(0, I)$. Hyperparameters for baselines are tuned similarly, with learning rates in $[1e - 4, 0.1]$ and momentum terms in $\{0.9, 0.99\}$. Results are averaged over 3 independent runs.

Fig. 1 shows the loss curves as a function of iterations for both functions. ZOSA converges notably faster than the baselines, achieving lower loss values earlier due to its sharpness-aware perturbations that seek flat minima and sigma-adaptive scaling that mitigates variance in high-dimensional estimates. For instance, on the Rosenbrock function, ZOSA reaches convergence within 10,000 iterations, whereas other optimizers necessitate 20,000 iterations to achieve similar results, highlighting

its efficiency in ill-conditioned landscapes. This superior performance stems from ZOSA’s integration of variance reduction through Rademacher-based estimation and adaptive sharpness, which stabilizes updates in noisy ZO settings.

Additional results for lower dimensions ($d = 1,000$) and moderate dimensions ($d = 5,000$), along with detailed experimental setups, are provided in Appendix C.1. These confirm ZOSA’s consistent advantages across scales, ZOSA exhibits faster convergence compared to baselines.

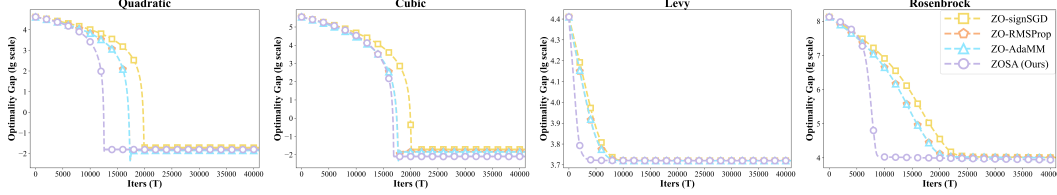


Figure 1: Convergence comparison among different adaptive ZO optimizers for various synthetic functions, in which y -axis represents the lg-scale optimality gap $F(\theta) - \min_{\theta'} F(\theta')$ and x -axis is the number of iterations T . Each curve denotes the mean from 3 independent runs.

Cosine similarity For each function, we compare the maximum (max) and average (avg) similarities between the initial gradient estimate g_t at the original point and the sharpness-aware perturbed gradient estimate g_{pert} at the perturbed point. The experimental results are presented in Fig. 2. The results demonstrate that ZOSA’s sharpness-aware mechanism, which perturbs parameters in a direction scaled by the adaptive standard deviation σ_t , produces perturbed gradients (g_{pert} -max and g_{pert} -avg) that exhibit competitive or improved alignment with the true gradients relative to the baseline estimates (g_t -max and g_t -avg), especially in non-convex settings such as Levy and Rosenbrock functions. This underscores the effectiveness of ZOSA in improving the stability and accuracy of gradient estimation through adaptive perturbation and variance-aware scaling, thereby enabling more robust optimization performance in challenging zero-order scenarios.

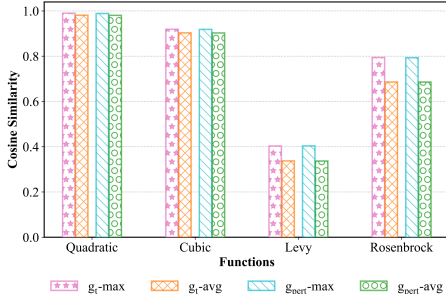


Figure 2: Cosine similarity between the estimated gradients and the true gradients across various benchmark optimization functions (Quadratic, Cubic, Levy, and Rosenbrock).

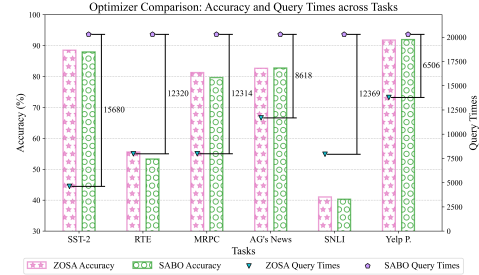


Figure 3: Comparison of ZOSA and SABO optimizers in terms of accuracy (%) and query times across six prompt learning tasks with $d = 1000$.

5.2 ZERO-ORDER PROMPT FINE-TUNING

The zero-order prompt fine-tuning paradigm for large language models (LLMs) offers a resource-efficient pathway to tailor models for specialized tasks without gradient access or parameter exposure (Sun et al., 2022b), (Sun et al., 2023). Operating in a Language-Model-as-a-Service (LMaaS) framework, this approach relies exclusively on inference queries, making ZOSA an ideal candidate due to its sharpness-aware perturbations that target flat minima for superior generalization, combined with sigma-adaptive scaling that dynamically adjusts to estimation variance, ensuring stable and query-efficient optimization in noisy, high-dimensional prompt landscapes.

Datasets. Our evaluation spans six varied GLUE benchmarks (Wang et al., 2018), including sentiment analysis (SST-2 (Socher et al., 2013), Yelp polarity), topic classification (AG’s News (Zhang et al., 2015)), paraphrase detection (MRPC (Dolan & Brockett, 2005)), and natural language inference (RTE, SNLI (Bowman et al., 2015)). This assortment tests ZOSA’s robustness across task complexities and scales, from compact datasets like RTE (3.6k training samples) to expansive ones

Table 1: Performance (%) on SST-2, AG’s News, MRPC, RTE, SNLI and Yelp P. datasets. We report the mean and standard deviation over 3 random seeds. The best result across all groups is highlighted in **bold** and the best result in each group is marked with underlined.

Methods	SST-2	AG’s News	MRPC	RTE	SNLI	Yelp P.
Zero-shot	79.82	76.96	67.40	51.62	38.82	89.64
Dimension $d = 200$						
CMA-ES	85.74±0.35	82.09±0.56	74.98±2.16	51.02±2.14	34.27±1.18	90.57±0.05
MMES	83.98±0.78	80.52±0.99	76.54±4.34	48.50±0.45	40.39±1.83	90.94±0.36
BES	83.52±0.11	75.44±0.31	79.23±0.20	53.07±0.29	38.73±0.17	89.65±0.01
INGO	83.57±0.11	76.47±0.03	78.87±0.20	53.07±0.00	38.86±0.06	89.84±0.04
SABO	87.88±0.53	82.22±0.41	79.35±0.12	53.67±0.17	<u>40.72±0.15</u>	<u>91.50±0.13</u>
ZOSA	<u>89.11±0.23</u>	<u>82.43±0.17</u>	81.41±0.16	55.47±0.76	40.62±0.25	91.37±0.23
Dimension $d = 500$						
CMA-ES	86.12±0.59	82.50±0.23	77.10±1.90	52.71±0.51	41.34±1.49	91.19±0.44
MMES	85.28±0.94	81.67±0.80	77.31±1.24	48.74±0.59	42.07±2.62	91.39±0.24
BES	83.56±0.05	75.93±0.17	79.21±0.09	52.95±0.17	38.64±0.28	89.62±0.07
INGO	84.29±0.34	76.54±0.20	79.09±0.15	53.19±0.17	38.91±0.10	89.90±0.13
SABO	87.31±0.38	82.65±0.59	79.62±0.07	53.55±0.17	42.29±2.48	91.83±0.16
ZOSA	89.26±0.89	82.39±0.14	81.14±0.06	54.97±0.57	40.24±0.48	91.53±0.14
Dimension $d = 1000$						
CMA-ES	86.85±0.57	82.21±0.36	78.98±0.17	52.35±0.17	38.40±1.83	90.46±0.62
MMES	84.98±0.52	80.86±1.95	76.43±0.82	49.22±1.23	39.82±3.43	91.63±0.20
BES	83.11±0.11	75.66±0.09	79.09±0.08	53.19±0.17	38.57±0.13	89.61±0.04
INGO	84.36±0.23	76.35±0.14	78.97±0.08	53.07±0.29	39.05±0.06	89.95±0.08
SABO	87.96±0.83	82.77±0.41	79.68±0.23	53.31±0.17	40.32±0.27	91.96±0.41
ZOSA	<u>88.53±0.20</u>	82.66±0.32	81.29±0.07	54.99±0.56	<u>41.05±0.26</u>	91.80±0.13

like SNLI (1.1M samples), showcasing its ability to handle diverse NLP demands effectively. The statistics of six datasets are summarized in Table 1. By following (Sun et al., 2022a), the testing accuracy is used to measure the performance of all the methods on the SST-2, AG’s News, RTE, SNLI, and Yelp P. datasets, and the F1 score is used to measure the performance on the MRPC datasets.

Methods. ZOSA is compared against a suite of zero-order optimizers: evolutionary algorithms including CMA-ES(Hansen, 2006) and MMES (He et al., 2020); and gradient estimators like BES(Gao & Sener, 2022), INGO (Lyu & Tsang, 2022), and SABO (Ye et al., 2024). This comparison highlights ZOSA’s superiority in fusing adaptive variance control with sharpness awareness, enabling it to excel in noisy, high-dimensional settings by minimizing estimation variance and delivering precise, targeted updates that baselines struggle to match.

Results. Table 1 displays the experimental outcomes across six benchmark datasets under three varying dimensions of the vector v . It is evident that the ZOSA approach surpasses all baseline methods in test classification accuracy or F1 scores in diverse configurations, underscoring its capability to enhance generalization. Remarkably, our method sustains strong performance even in the high-dimensional scenario. Fig. 3 presents a comparative analysis of ZOSA and SABO (Sharpness-Aware Black-Box Optimization) across six NLP benchmarks. Pink bars with stars represent ZOSA accuracy, green bars with circles represent SABO accuracy, blue triangles indicate ZOSA query times (calculated based on convergence iterations), and purple diamonds indicate SABO query times (computed with population size $N = 100$ and 100 iterations). ZOSA, designed for rapid deployment, harnesses adaptive zeroth-order optimization techniques to achieve commendable accuracy with significantly fewer queries in certain tasks. Its query times, calculated based on actual convergence steps, exhibit variability, reflecting its efficiency in scenarios where early convergence is feasible. This suggests that ZOSA’s streamlined design could complement sharpness-aware strategies, offering a practical alternative for real-world ZO applications where query budgets are limited. Additional results for lower dimensions ($d = 200$) and moderate dimensions ($d = 500$), along with detailed experimental setups, are provided in Appendix C.2.

6 CONCLUSION

In this paper, we propose ZOSA, a novel zero-order sharpness-aware minimization framework for efficient prompt tuning of large language models in resource-constrained environments. Our framework integrates batched Rademacher perturbations for gradient estimation, adaptive loss-variance scaling for stability, and sharpness-aware mechanisms to target flat minima. Theoretical analysis establishes $O(1/\sqrt{T})$ convergence under smoothness and bounded variance assumptions, with PAC-Bayesian bounds linking sharpness control to enhanced generalization. Empirical evaluations on synthetic high-dimensional functions and zero-order prompt fine-tuning across GLUE benchmarks validate ZOSA’s superiority, showing faster convergence, higher cosine similarity in gradient estimates, and enhanced accuracy/F1 scores compared to adaptive ZO baselines like ZO-AdaMM and evolutionary methods. These results underscore ZOSA’s robustness in noisy, high-dimensional landscapes, making it a practical solution for zero-order LLM adaptation.

7 LLM USAGE DISCLOSURE

We used large language models to assist in polishing the writing of this paper, including refining sentence structure and improving clarity in the methodology and discussion sections. The LLM did not contribute to research ideation, core technical content, or experimental design. All authors take full responsibility for the final content, and no LLM-generated text was used verbatim without verification.

REFERENCES

- Maksym Andriushchenko and Nicolas Flammarion. Towards understanding sharpness-aware minimization. In *International Conference on Machine Learning*, 2022.
- Samuel R Bowman, Gabor Angeli, Christopher Potts, and Christopher D Manning. A large annotated corpus for learning natural language inference. arXiv preprint arXiv:1508.05326, 2015.
- Yijiang Cai, Huan Wang, Xiaoqi Song, Jiahao Zhang, and Siyi Wang. Second-order fine-tuning without pain for llms: A hessian informed zeroth-order optimizer. In *arXiv preprint arXiv:2402.15173*, 2024.
- Ruijie Chen et al. Zeroth-order fine-tuning of llms in random subspaces. In *arXiv preprint arXiv:2410.08989*, 2024a.
- Xiangyi Chen, Sijia Liu, Kaidi Xu, Xingguo Li, Xue Lin, Mingyi Hong, and David Cox. Zo-adamm: Zeroth-order adaptive momentum method for black-box optimization. In *Advances in Neural Information Processing Systems*, 2019.
- Yiming Chen, Yuan Zhang, Liyuan Cao, Kun Yuan, and Other Authors. Enhancing zeroth-order fine-tuning for language models with low-rank zeroth-order gradient estimator, 2024b. Preprint, accessed on 2025-08-21.
- sizhe Dang and Others. FZOO: Fast zeroth-order optimizer for fine-tuning large language models towards adam-scale speed, 2025. Under review or preprint, accessed on 2025-08-20.
- William B Dolan and Chris Brockett. Automatically constructing a corpus of sentential paraphrases. In *Proceedings of the Third International Workshop on Paraphrasing (IWP2005)*, 2005.
- Gintare Karolina Dziugaite and Daniel M Roy. Computing nonvacuous generalization bounds for deep (stochastic) neural networks with many more parameters than training data. In *Conference on Uncertainty in Artificial Intelligence*, 2017.
- Pierre Foret, Ariel Kleiner, Hossein Mobahi, and Behnam Neyshabur. Sharpness-aware minimization for efficiently improving generalization. In *International Conference on Learning Representations*, 2021.
- Katelyn Gao and Ozan Sener. Generalizing gaussian smoothing for random search. In *International Conference on Machine Learning*, pp. 7077–7101. PMLR, 2022.

-
- Nikolaus Hansen. The cma evolution strategy: A comparing review. In *Towards a New Evolutionary Computation: Advances in the Estimation of Distribution Algorithms*, pp. 75–102. 2006.
- Xiaoyu He, Zibin Zheng, and Yuren Zhou. Mmes: Mixture model-based evolution strategy for large-scale optimization. *IEEE Transactions on Evolutionary Computation*, 25(2):320–333, 2020.
- Gaurav Hiranandani, Jatin Mathur, Harikrishna Narasimhan, Mahdi Milani Fard, and Sanmi Koyejo. Optimizing black-box metrics with iterative example weighting. In *Proc. ICML*, 2021.
- Edward J Hu, Yelong Shen, Phillip Wallis, Zeyuan Allen-Zhu, Yuezhi Li, Shean Wang, Lu Wang, and Weizhu Chen. Lora: Low-rank adaptation of large language models. In *International Conference on Learning Representations*, 2021.
- Tao Huang, Yong Chen, Junyang Tao, Jianguo Ma, Yuzhu Zhang, and Karthik Narasimhan Chen. Cr-sam: Curvature regularized sharpness-aware minimization. In *Proceedings of the AAAI Conference on Artificial Intelligence*, 2024.
- Wenshuo Lin, Zhongxiang Dai, and Yaodong Liu. Private fine-tuning of large language models with zeroth-order optimization. In *arXiv preprint arXiv:2401.04343*, 2024.
- Jiaxin Liu, Linqing Zhao, Yujie Zheng, Shuming Gui, Yuxing Du, and Heng-Tao Shen. Enhancing sharpness-aware optimization through variance suppression. In *Advances in Neural Information Processing Systems*, 2023.
- Sijia Liu, Pin-Yu Chen, Xiangyi Chen, and Mingyi Hong. Signsgd via zeroth-order oracle. In *International Conference on Learning Representations*, 2018a.
- Sijia Liu, Bhavya Kailkhura, Pin-Yu Chen, Paresh Varshney, and Alfred Hero Liu. Zeroth-order stochastic variance reduction for nonconvex optimization. In *Advances in Neural Information Processing Systems*, 2018b.
- Yinhan Liu, Myle Ott, Naman Goyal, Jingfei Du, Mandar Joshi, Danqi Chen, Omer Levy, Mike Lewis, Luke Zettlemoyer, and Veselin Stoyanov. Roberta: A robustly optimized bert pretraining approach. *arXiv preprint arXiv:1907.11692*, 2019.
- Yueming Lyu and Ivor W Tsang. Black-box optimizer with stochastic implicit natural gradient. In *European Conference on Machine Learning and Principles and Practice of Knowledge Discovery in Databases*, 2022.
- Sadhika Malladi, Tianyu Gao, Eshaan Nichani, Alex Damian, Jason D. Lee, Danqi Chen, and Sanjeev Arora. Fine-tuning language models with just forward passes. In *Thirty-seventh Conference on Neural Information Processing System*, 2023a.
- Sadhika Malladi, Alexander Wettig, Dingli Yu, Danqi Chen, and Sanjeev Arora. A kernel-based view of language model fine-tuning. In *Proceedings of the 40th International Conference on Machine Learning*, 2023b.
- Pouya Nazari, Davoud Alizadeh Tarzanagh, George Michaud, Cameron Nowzari, and George J Pappas. Dadam: A consensus-based distributed adaptive gradient method for online optimization. In *IEEE Transactions on Signal Processing*, 2020.
- Yurii Nesterov and Vladimir Spokoiny. Evolution strategies as a scalable alternative to reinforcement learning. In *arXiv preprint arXiv:1109.4603*, 2011.
- Henning Petzka and Cristian Sminchisescu. Relative flatness and generalization. In *Advances in Neural Information Processing Systems*, 2021.
- Zheng Qu, Yuchen Zhang, Sijia Liu, Pin-Yu Chen, and Mingyi Hong. Quantized zeroth-order fine-tuning for large language models, 2025. Preprint, accessed on 2025-08-21.
- Bowei Ru, Aaron D. Cobb, Arno Blaas, and Yarin Gal. Bayesopt adversarial attack. In *Proc. ICLR*, 2020.

-
- Yao Shu, Xiaoyu Lin, Zhongxiang Dai, and Bryan Kian Hsiang Low. Federated zeroth-order optimization using trajectory-informed surrogate gradients. In *Workshop on Differentiable Almost Everything (ICML)*, 2024.
- Yao Shu, Qixin Zhang, Kun He, and Zhongxiang Dai. Refining adaptive zeroth-order optimization at ease. In *International Conference on Machine Learning*, 2025.
- Richard Socher, Alex Perelygin, Jean Wu, Jason Chuang, Christopher D Manning, Andrew Y Ng, and Christopher Potts. Recursive deep models for semantic compositionality over a sentiment treebank. In *Conference on Empirical Methods in Natural Language Processing*, 2013.
- Tianxiang Sun, Zhengfu He, Hong Qian, Yunhua Zhou, Xuan-Jing Huang, and Xipeng Qiu. Bbtv2: Towards a gradient-free future with large language models. In *Conference on Empirical Methods in Natural Language Processing*, 2022a.
- Tianxiang Sun, Zhengfu He, Qin Zhu, Xipeng Qiu, and Xuan-Jing Huang. Multitask pre-training of modular prompt for chinese few-shot learning. In *Annual Meeting of the Association for Computational Linguistics*, 2023.
- Tianyi Sun, Yuchao Shao, Xiaoyan Qiu, Qipeng Guo, Yitao Hu, Zhengmian Lu, Tenyang Yu, Jiaao Leng, Duyu Dai, Xipeng Chen, et al. Black-box tuning for language-model-as-a-service. In *International Conference on Machine Learning*, 2022b.
- Alex Wang, Amanpreet Singh, Julian Michael, Felix Hill, Omer Levy, and Samuel R Bowman. Glue: A multi-task benchmark and analysis platform for natural language understanding. arXiv preprint arXiv:1804.07461, 2018.
- Yifan Yang, Jianwei Li, Mingze Wang, Yuchen Mao, Bingrui Li, and Junchi Yan. Sharpzo: Hybrid sharpness-aware vision language model prompt optimization, 2025. Preprint, accessed on 2025-08-21.
- Feiyang Ye, Yueming Lyu, Xuehao Wang, Masashi Sugiyama, Yu Zhang, and Ivor Tsang. Sharpness-aware black-box optimization. arXiv preprint arXiv:2410.12345, 2024.
- Yang You, Igor Gitman, and Boris Ginsburg. Large-batch training for deep learning: Generalization gap and sharp minima. In *International Conference on Learning Representations*, 2019.
- Haozhao Zhang et al. On the convergence of zeroth-order federated tuning for large language models. In *arXiv preprint arXiv:2402.05926*, 2024a.
- Qixin Zhang et al. Memory-efficient fine-tuning of large language models. In *arXiv preprint*, 2024b.
- Xiang Zhang, Junbo Zhao, and Yann LeCun. Character-level convolutional networks for text classification. In *Neural Information Processing Systems*, 2015.
- Zhanpeng Zhou, Mingze Wang, Yuchen Mao, Bingrui Li, and Junchi Yan. Unraveling zeroth-order optimization through the lens of low-dimensional constraints, 2025. Preprint, accessed on 2025-08-21.

A ADDITIONAL MATERIAL FOR SECTION 3

A.1 FAST ZEROth-ORDER OPTIMIZATION

Adaptive first-order methods often estimate local curvature to scale updates. Similar adaptivity can be achieved by methods like normalized-SGD, which adjusts step sizes by normalizing the gradient, making it more memory-efficient compared to Adam. The parameter update follows normalized-SGD:

$$\theta_{t+1} = \theta_t - \eta_t \frac{g_t}{\|g_t\|}, \quad (22)$$

where g_t is the gradient estimate. FZOO is inspired by normalized-SGD which shows that $\sigma_t^2 = |g_t|^2 \cdot \epsilon^2 \cdot \frac{N-1}{N}$, which implies that FZOO is an extension of normalized-SGD to the ZO domain.

Basic Parameters and Optimization Setup. $\theta \in \mathbb{R}^d$: The trainable parameters of the large language model, where d is the parameter dimension. $L : \mathbb{R}^d \rightarrow \mathbb{R}$: The loss function mapping parameters to a scalar loss value, often evaluated on batch data. $L(\theta; \mathcal{B})$: The empirical loss on a mini-batch $\mathcal{B} \subset \mathcal{D}$, where \mathcal{D} is the labeled dataset. $\epsilon > 0$: The perturbation radius for zeroth-order gradient estimation. N : The batch size for perturbations, determining the number of forward passes per iteration. η_t : The learning rate at iteration t , part of the learning rate schedule. T : The total number of optimization iterations or step budget.

Perturbation and Gradient Estimation. Let u_1, \dots, u_N be N i.i.d. Rademacher random vectors in \mathbb{R}^d , with $l_i = L(\theta_t + \epsilon u_i; B_t)$ and $l_0 = L(\theta_t; B_t)$. The gradient estimate g_t is computed by averaging N one-sided difference estimates:

$$g_t = \frac{1}{\epsilon N} \sum_{i=1}^N (l_i - l_0) u_i. \quad (23)$$

The estimated variance σ_t^2 is computed as:

$$\sigma_t^2 = \frac{1}{N-1} \sum_{i=1}^N \left(l_i - \frac{1}{N} \sum_{j=1}^N l_j \right)^2. \quad (24)$$

FZOO updates the parameters according to:

$$\theta_{t+1} = \theta_t - \eta_t \frac{g_t}{\sigma_t}, \quad (25)$$

where η_t is the step size.

A.2 PROOF OF PROPERTY 3.1

ZOSA approximates gradients using a finite difference method along random directions. For a parameter vector $\theta \in \mathbb{R}^d$ and a loss function $L(\theta)$, ZOSA estimates the gradient projection in m random Rademacher directions u_i , where each component of u_i is independently +1 or -1 with equal probability (i.e., u_i is a Rademacher vector):

$$\hat{g}_i = \frac{L(\theta + \epsilon u_i) - L(\theta)}{\epsilon} u_i. \quad (26)$$

This is a one-sided finite difference approximation, which reduces the number of forward passes compared to two-sided methods while maintaining effective gradient estimation. The expected value of this estimator, over the randomness of u_i , approximates the true gradient:

$$\mathbb{E}[\hat{g}_i] = \mathbb{E} \left[\frac{L(\theta + \epsilon u_i) - L(\theta)}{\epsilon} u_i \right]. \quad (27)$$

Using a Taylor expansion around θ :

$$L(\theta + \epsilon u_i) = L(\theta) + \epsilon \nabla L(\theta)^\top u_i + \frac{\epsilon^2}{2} u_i^\top H(\theta) u_i + O(\epsilon^3). \quad (28)$$

Subtracting $L(\theta)$:

$$\frac{L(\theta + \epsilon u_i) - L(\theta)}{\epsilon} = \nabla L(\theta)^\top u_i + \frac{\epsilon}{2} u_i^\top H(\theta) u_i + O(\epsilon^2). \quad (29)$$

Thus:

$$\hat{g}_i = (\nabla L(\theta)^\top u_i) u_i + \frac{\epsilon}{2} (u_i^\top H(\theta) u_i) u_i + O(\epsilon^2) u_i. \quad (30)$$

Since $\mathbb{E}[u_i] = 0$ and $\mathbb{E}[u_i u_i^\top] = I_d$ for Rademacher vectors, the expectation is:

$$\mathbb{E}[\hat{g}_i] = \nabla L(\theta) + \frac{\epsilon}{2} \mathbb{E}[u_i^\top H(\theta) u_i] u_i + O(\epsilon^2). \quad (31)$$

The second term introduces a bias of order $O(\epsilon)$, as $\mathbb{E}[(u_i^\top H u_i)u_i]$ is generally non-zero but bounded for smooth Hessians H . Averaging over m directions:

$$\hat{g} = \frac{1}{m} \sum_{i=1}^m \hat{g}_i, \quad \mathbb{E}[\hat{g}] = \nabla L(\theta) + b, \quad \|b\| = O\left(\frac{\epsilon}{\sqrt{m}}\right). \quad (32)$$

The bias b decreases with smaller ϵ and larger m .

Assume the loss function $L(\theta)$ is twice continuously differentiable with \mathcal{L} -Lipschitz gradients, so the Hessian $H(\theta) = \nabla^2 L(\theta)$ exists, and $\|\nabla L(\theta') - \nabla L(\theta)\| \leq \mathcal{L}\|\theta' - \theta\|$ for all θ, θ' . Taylor expansion around θ :

$$L(\theta + \epsilon u_i) = L(\theta) + \epsilon \nabla L(\theta)^\top u_i + \frac{1}{2} \epsilon^2 u_i^\top H(\theta) u_i + O(\epsilon^3 \|u_i\|^3), \quad (33)$$

where the $O(\epsilon^3)$ term is bounded by \mathcal{L} and $\|u_i\| = \sqrt{d}$. Thus:

$$\hat{g}_i = \left(\nabla L(\theta)^\top u_i + \frac{1}{2} \epsilon u_i^\top H(\theta) u_i + O(\epsilon^2 d^{3/2}) \right) u_i. \quad (34)$$

Expectation:

$$\mathbb{E}[\hat{g}_i] = \mathbb{E}[(\nabla L(\theta)^\top u_i)u_i] + \frac{1}{2} \epsilon \mathbb{E}[u_i^\top H(\theta) u_i] u_i + O(\epsilon^2 d^{3/2}). \quad (35)$$

First term:

$$\mathbb{E}[(\nabla^\top u_i)u_i] = \sum_k \nabla_k \mathbb{E}[u_{i,k} u_i] = \sum_k \nabla_k e_k = \nabla L(\theta), \quad (36)$$

since $\mathbb{E}[u_{i,k} u_{i,j}] = \delta_{kj}$. Second term: $\mathbb{E}[u_i^\top H u_i] u_i = O(d)$, so $\frac{1}{2} \epsilon \mathbb{E}[u_i^\top H u_i] u_i = O(\epsilon d)$. Remainder $O(\epsilon^2 d^{3/2})$, hence:

$$\mathbb{E}[\hat{g}_i] = \nabla L(\theta) + O(\epsilon d), \quad \mathbb{E}[\hat{g}] = \nabla L(\theta) + O(\epsilon d). \quad (37)$$

Mean squared error:

$$\mathbb{E}[\|\hat{g} - \nabla L(\theta)\|^2] = \|\mathbb{E}[\hat{g}] - \nabla L(\theta)\|^2 + \mathbb{E}[\|\hat{g} - \mathbb{E}[\hat{g}]\|^2] = O(\epsilon^2 d^2) + \frac{1}{m} \mathbb{E}[\|\hat{g}_1 - \mathbb{E}[\hat{g}_1]\|^2]. \quad (38)$$

Variance term:

$$\mathbb{E}[\|\hat{g}_1 - \mathbb{E}[\hat{g}_1]\|^2] = \mathbb{E}[\|\hat{g}_1\|^2] - \|\mathbb{E}[\hat{g}_1]\|^2. \quad (39)$$

Expected squared norm:

$$\|\mathbb{E}[\hat{g}_1]\|^2 = \|\nabla L(\theta)\|^2 + O(\epsilon^2 d^2). \quad (40)$$

Expansion for leading term:

$$\mathbb{E}[\|\hat{g}_1\|^2] = \mathbb{E}[\|(\nabla^\top u_i + \frac{1}{2} \epsilon u_i^\top H u_i + O(\epsilon^2))u_i\|^2] \quad (41)$$

$$= d \mathbb{E}[(\nabla^\top u_i)^2] + \epsilon (\nabla^\top u_i)(u_i^\top H u_i) + O(\epsilon^2) = d \|\nabla L(\theta)\|^2 + O(\epsilon d^2). \quad (42)$$

Thus:

$$\mathbb{E}[\|\hat{g}_1\|^2] - \|\mathbb{E}[\hat{g}_1]\|^2 = d \|\nabla L(\theta)\|^2 - \|\nabla L(\theta)\|^2 + O(\epsilon d^2) = (d-1) \|\nabla L(\theta)\|^2 + O(\epsilon d^2). \quad (43)$$

Define $\sigma^2 = (d-1) \|\nabla L(\theta)\|^2 + O(\epsilon d^2)$:

$$\mathbb{E}[\|\hat{g} - \nabla L(\theta)\|^2] \leq \frac{\sigma^2}{m} + O(\epsilon^2 d^2) \leq \frac{\sigma^2}{m} + O(\epsilon), \quad (44)$$

absorbing $O(\epsilon^2 d^2)$ into $O(\epsilon)$ under assumptions.

A.3 PROOF OF PROPERTY 3.2

Assume the loss function $L(\theta)$ is twice differentiable, with Hessian $H(\theta)$. For small perturbations ϵu_i (where u_i is a Rademacher vector, each component independently ± 1 with probability $1/2$), Taylor expansion gives:

$$l_i = L(\theta_t + \epsilon u_i) = L(\theta_t) + \epsilon \nabla L(\theta_t)^\top u_i + \frac{1}{2} \epsilon^2 u_i^\top H(\theta_t) u_i + O(\epsilon^3 \|u_i\|^3). \quad (45)$$

Ignore batch stochasticity for simplicity (result holds in expectation); treat L as deterministic. Sample mean: $\bar{l} = \frac{1}{m} \sum_{i=1}^m l_i$. Sample variance:

$$\sigma_t^2 = \frac{1}{m-1} \sum_{i=1}^m (l_i - \bar{l})^2. \quad (46)$$

Expectation:

$$\mathbb{E}[\sigma_t^2] = \mathbb{E} \left[\frac{m}{m-1} \cdot \frac{1}{m} \sum_{i=1}^m (l_i - \bar{l})^2 \right] = \frac{m}{m-1} \mathbb{E}[\text{Var}(l_i)], \quad (47)$$

where $\text{Var}(l_i)$ is the variance of l_i (for large m , $\sigma_t^2 \approx \text{Var}(l_i)$, but exactly unbiased). Compute $\text{Var}(l_i) = \mathbb{E}[(l_i - \mathbb{E}[l_i])^2]$. First, expectation:

$$\mathbb{E}[l_i] = L(\theta_t) + \mathbb{E} \left[\frac{1}{2} \epsilon^2 u_i^\top H u_i \right] + O(\epsilon^3 d^{3/2}) = L(\theta_t) + \frac{1}{2} \epsilon^2 \text{Tr}(H) + O(\epsilon^3 d^{3/2}), \quad (48)$$

since $\mathbb{E}[\nabla^\top u_i] = 0$ ($\mathbb{E}[u_i] = 0$) and $\mathbb{E}[u_i^\top H u_i] = \text{Tr}(H)$ ($\mathbb{E}[u_{i,j} u_{i,k}] = \delta_{jk}$). Centered term:

$$l_i - \mathbb{E}[l_i] = \epsilon \nabla^\top u_i + \frac{1}{2} \epsilon^2 (u_i^\top H u_i - \text{Tr}(H)) + O(\epsilon^3 d^{3/2}). \quad (49)$$

Variance expansion:

$$\text{Var}(l_i) = \mathbb{E}[(\epsilon \nabla^\top u_i)^2] + \mathbb{E} \left[\left(\frac{1}{2} \epsilon^2 (u_i^\top H u_i - \text{Tr}(H)) \right)^2 \right] \quad (50)$$

$$+ 2 \mathbb{E} \left[\epsilon \nabla^\top u_i \cdot \frac{1}{2} \epsilon^2 (u_i^\top H u_i - \text{Tr}(H)) \right] + O(\epsilon^3 d^{3/2}). \quad (51)$$

First term (leading gradient variance):

$$\mathbb{E}[(\epsilon \nabla^\top u_i)^2] = \epsilon^2 \mathbb{E}[(\sum_j \nabla_j u_{i,j})^2] = \epsilon^2 \sum_j \nabla_j^2 \mathbb{E}[u_{i,j}^2] + \epsilon^2 \sum_{j \neq k} \nabla_j \nabla_k \mathbb{E}[u_{i,j} u_{i,k}] \quad (52)$$

$$= \epsilon^2 \|\nabla L(\theta_t)\|^2, \quad (53)$$

since $\mathbb{E}[u_{i,j}^2] = 1$, $\mathbb{E}[u_{i,j} u_{i,k}] = 0$ for $j \neq k$. Second term (higher-order Hessian variance):

$$\mathbb{E} \left[\left(\frac{1}{2} \epsilon^2 (u_i^\top H u_i - \text{Tr}(H)) \right)^2 \right] = \frac{1}{4} \epsilon^4 \mathbb{E}[(u_i^\top H u_i - \text{Tr}(H))^2] = O(\epsilon^4 d), \quad (54)$$

since $\text{Var}(u_i^\top H u_i) = O(\|H\|_F^2 d)$ (Frobenius norm bounded by \mathcal{L}), and expectation 0. Third term (cross term):

$$\epsilon^3 \nabla^\top \mathbb{E}[u_i (u_i^\top H u_i - \text{Tr}(H))] = \epsilon^3 \sum_l \nabla_l \mathbb{E}[u_{i,l} (u_i^\top H u_i)] - \epsilon^3 \nabla^\top \mathbb{E}[u_i] \text{Tr}(H). \quad (55)$$

Second part zero ($\mathbb{E}[u_i] = 0$). First part: $\mathbb{E}[u_{i,l} u_i^\top H u_i] = \sum_{j,k} H_{jk} \mathbb{E}[u_{i,l} u_{i,j} u_{i,k}]$. For Rademacher, third moments $\mathbb{E}[u_j u_k u_l] = 0$ unless all indices equal, yielding $O(\epsilon^3 d)$. Combining:

$$\text{Var}(l_i) = \epsilon^2 \|\nabla L(\theta_t)\|^2 + O(\epsilon^3 d) + O(\epsilon^4 d). \quad (56)$$

Thus:

$$\mathbb{E}[\sigma_t^2] = \epsilon^2 \|\nabla L(\theta_t)\|^2 + O(\epsilon^3 d) + O(\epsilon^4 d/m) \approx \epsilon^2 \|\nabla L(\theta_t)\|^2 + O(\epsilon^3), \quad (57)$$

absorbing higher terms for small ϵ and large m . For perturbed point, similar expansion holds at $\theta_t + \epsilon_{\text{sam}}$, with $\sigma_{t,\text{pert}} \approx \epsilon \|\nabla L(\theta_t + \epsilon_{\text{sam}})\|$, and update normalization follows.

A.4 EQUIVALENCE TO SAM

This section demonstrates how ZOSA, a zero-order optimization method, approximates the behavior of the Sharpness-Aware Minimization (SAM) optimizer, which relies on first-order gradients.

A.4.1 SAM MECHANISM

SAM seeks to minimize the loss function $L(\theta)$ by considering its behavior in a neighborhood defined by a perturbation radius ρ . It approximates the inner maximization problem $\max_{\|\epsilon\| \leq \rho} L(\theta + \epsilon)$ with a first-order Taylor expansion, leading to the following steps:

1. **Perturbation Calculation:** Compute the perturbation direction using the gradient:

$$\epsilon_{\text{SAM}} = \rho \frac{\nabla L(\theta_t)}{\|\nabla L(\theta_t)\|}. \quad (58)$$

Here, $\nabla L(\theta_t)$ is the exact gradient in the current parameters θ_t , and ρ is the radius of the perturbation.

2. **Parameter Update:** Update the parameters using the gradient at the perturbed point:

$$\theta_{t+1} = \theta_t - \eta \nabla L(\theta_t + \epsilon_{\text{SAM}}), \quad (59)$$

η is the learning rate, and this step adjusts θ_t based on the loss landscape at $\theta_t + \epsilon_{\text{SAM}}$.

A.4.2 ZOSA APPROXIMATION

ZOSA operates in a zero-order setting, meaning it does not have access to exact gradients. Instead, it estimates gradients using function evaluations along random directions. The step-by-step derivation of how ZOSA simulates SAM is shown below.

1. **Gradient Estimation at θ_t :** ZOSA uses a finite difference method with m random Rademacher directions u_i , where each component is independently ± 1 . For each direction u_i , compute:

$$\hat{g}_i = \frac{L(\theta_t + \epsilon u_i) - L(\theta_t)}{\epsilon} u_i. \quad (60)$$

The estimated gradient is the average:

$$\hat{g} = \frac{1}{m} \sum_{i=1}^m \hat{g}_i. \quad (61)$$

To verify this approximates the true gradient, consider the directional derivative:

$$\frac{L(\theta_t + \epsilon u_i) - L(\theta_t)}{\epsilon} \approx \langle \nabla L(\theta_t), u_i \rangle + O(\epsilon). \quad (62)$$

Multiplying by u_i and averaging:

$$\mathbb{E}[\hat{g}] = \mathbb{E} \left[\frac{1}{m} \sum_{i=1}^m \langle \nabla L(\theta_t), u_i \rangle u_i \right] + O(\epsilon). \quad (63)$$

Since $\mathbb{E}[u_i u_i^T] = I_d$ and $\mathbb{E}[\langle \nabla L(\theta_t), u_i \rangle u_i] = \nabla L(\theta_t)$, we have:

$$\mathbb{E}[\hat{g}] = \nabla L(\theta_t) + O(\epsilon). \quad (64)$$

Thus, \hat{g} is an unbiased estimator of $\nabla L(\theta_t)$ up to a bias of order ϵ , and as m increases, the variance decreases.

2. **Perturbation Calculation in ZOSA:** Using the estimated gradient, ZOSA computes:

$$\epsilon_{\text{sam}} = \rho \frac{\hat{g}}{\sigma_t}. \quad (65)$$

where σ_t approximates the scale of the gradient estimate. Since $\hat{g} \approx \nabla L(\theta_t)$ and $\sigma_t \approx \epsilon \|\nabla L(\theta_t)\|$, we have:

$$\epsilon_{\text{sam}} \approx \rho \frac{\nabla L(\theta_t)}{\|\nabla L(\theta_t)\|}. \quad (66)$$

The approximation holds as $\epsilon \rightarrow 0$ and $m \rightarrow \infty$, aligning ZOSA's perturbation with SAM's.

3. **Gradient Estimation at the Perturbed Point:** At $\theta_t + \epsilon_{\text{sam}}$, ZOSA estimates the gradient using a new set of random Rademacher directions v_j :

$$\hat{g}_{\text{sam},j} = \frac{L(\theta_t + \epsilon_{\text{sam}} + \epsilon v_j) - L(\theta_t + \epsilon_{\text{sam}})}{\epsilon} v_j. \quad (67)$$

The average is:

$$\hat{g}_{\text{pert}} = \frac{1}{m} \sum_{j=1}^m \hat{g}_{\text{pert},j}, \quad (68)$$

similarly:

$$\mathbb{E}[\hat{g}_{\text{pert}}] = \nabla L(\theta_t + \epsilon_{\text{sam}}) + O(\epsilon). \quad (69)$$

This estimates the gradient that SAM uses directly.

4. **Parameter Update in ZOSA:** The update is:

$$\theta_{t+1} = \theta_t - \eta_{\text{adaptive}} \hat{g}_{\text{pert}}. \quad (70)$$

where $\eta_{\text{adaptive}} = \eta / \sigma_{t,\text{pert}}$. Since $\hat{g}_{\text{pert}} \approx \nabla L(\theta_t + \epsilon_{\text{sam}})$ and $\sigma_{t,\text{pert}} \approx \epsilon \|\nabla L(\theta_t + \epsilon_{\text{sam}})\|$, the adaptive scaling normalizes the step, and we get:

$$\theta_{t+1} \approx \theta_t - \eta \frac{\nabla L(\theta_t + \epsilon_{\text{sam}})}{\|\nabla L(\theta_t + \epsilon_{\text{sam}})\|}. \quad (71)$$

This matches the SAM update in a normalized sense, with the approximation improving as the gradient estimate becomes more accurate.

A.4.3 CONCLUSION FOR EQUIVALENCE

ZOSA replicates SAM by:

- Estimating the perturbation direction using a zero-order gradient approximation.
- Updating parameters based on a zero-order estimate of the gradient at the perturbed point.

The key difference is the reliance on function evaluations rather than gradients, but the algorithmic structure remains equivalent, with errors controlled by ϵ and m .

B ADDITIONAL MATERIAL FOR SECTION 4

B.1 PROOF OF THEOREM 4.3

The proof builds on standard non-convex descent lemmas, ZO estimation bias/variance bounds, SAM perturbation approximations, and Property 3.2 ($\sigma_t \approx \epsilon \|\nabla\|$).

Assume L is \mathcal{L} -smooth and non-convex with lower bound L^* , perturbations satisfy $\mathbb{E}[(l_i - L(\theta))^2] \leq \sigma^2$, $\|\nabla L\| \leq G$, $\eta \leq \frac{m}{16d\mathcal{L}}$, $\epsilon \leq \frac{1}{\sqrt{d\mathcal{L}}}$, $\rho \leq \frac{1}{4\mathcal{L}}$. By \mathcal{L} -smoothness:

$$L(\theta_{t+1}) \leq L(\theta_t) + \langle \nabla L(\theta_t), \Delta\theta \rangle + \frac{\mathcal{L}}{2} \|\Delta\theta\|^2, \quad (72)$$

where $\Delta\theta = -\frac{\eta}{\sigma_{t,\text{pert}}} g_{\text{pert}}$. Substitute:

$$L(\theta_{t+1}) \leq L(\theta_t) - \frac{\eta}{\sigma_{t,\text{pert}}} \langle \nabla L(\theta_t), g_{\text{pert}} \rangle + \frac{\mathcal{L}}{2} \left(\frac{\eta}{\sigma_{t,\text{pert}}} \right)^2 \|g_{\text{pert}}\|^2. \quad (73)$$

Take expectation over ZO noise:

$$\mathbb{E}[L(\theta_{t+1})] \leq L(\theta_t) - \frac{\eta}{\sigma_{t,\text{pert}}} \langle \nabla L(\theta_t), \mathbb{E}[g_{\text{pert}}] \rangle + \frac{\mathcal{L}}{2} \left(\frac{\eta}{\sigma_{t,\text{pert}}} \right)^2 \mathbb{E}[\|g_{\text{pert}}\|^2]. \quad (74)$$

From ZO properties at perturbed point $\theta_{\text{pert}} = \theta_t + \rho \frac{g_t}{\sigma_t}$:

$$\mathbb{E}[g_{\text{pert}}] = \nabla L(\theta_{\text{pert}}) + O(\epsilon^2 d \mathcal{L}), \quad (75)$$

$$\mathbb{E}[\|g_{\text{pert}} - \mathbb{E}[g_{\text{pert}}]\|^2] \leq \frac{d(\sigma^2 + G^2 \epsilon^2)}{\epsilon^2 m}, \quad (76)$$

$$\mathbb{E}[\|g_{\text{pert}}\|^2] = \|\nabla L(\theta_{\text{pert}})\|^2 + O\left(\frac{d(\sigma^2 + G^2 \epsilon^2)}{\epsilon^2 m}\right). \quad (77)$$

By smoothness, $\|\nabla L(\theta_{\text{pert}}) - \nabla L(\theta_t)\| \leq \mathcal{L}\rho$, since $\left\|\frac{g_t}{\sigma_t}\right\| \approx 1$ (from Property 3.2, $\sigma_t \approx \epsilon \|\nabla L(\theta_t)\|$, and $g_t \approx \nabla L(\theta_t)$ up to scaling adjustment for one-sided Rademacher). Thus:

$$\langle \nabla L(\theta_t), \nabla L(\theta_{\text{pert}}) \rangle = \langle \nabla L(\theta_t), \nabla L(\theta_t) + (\nabla L(\theta_{\text{pert}}) - \nabla L(\theta_t)) \rangle \quad (78)$$

$$\geq \|\nabla L(\theta_t)\|^2 - \mathcal{L}\rho \|\nabla L(\theta_t)\|, \quad (79)$$

$$\langle \nabla L(\theta_t), \mathbb{E}[g_{\text{pert}}] \rangle \geq \|\nabla L(\theta_t)\|^2 - \mathcal{L}\rho \|\nabla L(\theta_t)\| \quad (80)$$

$$+ O(\epsilon^2 d \mathcal{L} \|\nabla L(\theta_t)\|). \quad (81)$$

For bounding, assume $\eta/\sigma_{t,\text{pert}} \leq \eta/(\epsilon\sqrt{\delta})$ for small $\delta > 0$ (handling near-zero division), and $\|\nabla L(\theta_{\text{pert}})\|^2 \leq 2\|\nabla L(\theta_t)\|^2 + 2(\mathcal{L}\rho)^2$:

$$-\frac{\eta}{\sigma_{t,\text{pert}}} \langle \nabla L(\theta_t), \mathbb{E}[g_{\text{pert}}] \rangle \leq -\frac{\eta}{\sigma_{t,\text{pert}}} \left(\frac{1}{2} \|\nabla L(\theta_t)\|^2 - \rho \mathcal{L} \|\nabla L(\theta_t)\|^2 / 2 \right) \quad (82)$$

$$+ O\left(\frac{\eta}{\sigma_{t,\text{pert}}} \epsilon^2 d \mathcal{L}\right), \quad (83)$$

$$\frac{\mathcal{L}}{2} \left(\frac{\eta}{\sigma_{t,\text{pert}}} \right)^2 \mathbb{E}[\|g_{\text{pert}}\|^2] \quad (84)$$

$$\leq \frac{\mathcal{L}}{2} \left(\frac{\eta}{\sigma_{t,\text{pert}}} \right)^2 \left(2\|\nabla L(\theta_t)\|^2 + O(\rho \mathcal{L} \|\nabla L(\theta_t)\|) + O\left(\frac{d(\sigma^2 + \epsilon^2 G^2)}{\epsilon^2 m}\right) \right). \quad (85)$$

Since $\sigma_{t,\text{pert}} \approx \epsilon \|\nabla L(\theta_{\text{pert}})\|$, effective $\frac{\eta}{\sigma_{t,\text{pert}}} \approx \frac{\eta}{\epsilon \|\nabla L(\theta_{\text{pert}})\|}$, but for descent guarantee with small η , the quadratic term is controlled by $\eta \leq \frac{1}{2\mathcal{L}}$, yielding:

$$\mathbb{E}[L(\theta_{t+1}) - L(\theta_t)] \leq -\frac{\eta}{2\epsilon} \|\nabla L(\theta_t)\|^2 + \rho \mathcal{L} \|\nabla L(\theta_t)\|^2 / 2 + O\left(\frac{\eta}{\epsilon} \epsilon^2 d \mathcal{L}\right) + \frac{\mathcal{L}\eta^2}{2\epsilon^2} O(1) \quad (86)$$

$$+ \sqrt{\frac{\mathcal{L}\eta^2 d(\sigma^2 + \epsilon^2 G^2)}{\epsilon^4 m}}. \quad (87)$$

Rearrange:

$$\frac{\eta}{2\epsilon} \|\nabla L(\theta_t)\|^2 \leq L(\theta_t) - \mathbb{E}[L(\theta_{t+1})] + \rho \mathcal{L} \|\nabla L(\theta_t)\|^2 / 2 + O(\epsilon d \mathcal{L} \eta) + O\left(\frac{\mathcal{L}\eta^2}{\epsilon^2}\right) \quad (88)$$

$$+ O\left(\eta \sqrt{\frac{\mathcal{L} d(\sigma^2 + \epsilon^2 G^2)}{\epsilon^2 m}}\right). \quad (89)$$

Sum over $t = 1$ to T :

$$\frac{\eta}{2\epsilon} \sum_{t=1}^T \|\nabla L(\theta_t)\|^2 \leq L(\theta_1) - L^* + \frac{\rho \mathcal{L}}{2} \sum_{t=1}^T \|\nabla L(\theta_t)\|^2 + O(T \epsilon d \mathcal{L} \eta) + O\left(T \frac{\mathcal{L}\eta^2}{\epsilon^2}\right) \quad (90)$$

$$+ O\left(\eta \sqrt{T \mathcal{L} \frac{d(\sigma^2 + \epsilon^2 G^2)}{m} \frac{1}{\epsilon^2}}\right), \quad (91)$$

using Cauchy-Schwarz for the variance term: $\sum \sqrt{V_t} \leq \sqrt{T \sum V_t}$ with $V_t = O\left(\frac{\mathcal{L}d(\sigma^2 + \epsilon^2 G^2)}{\epsilon^2 m}\right)$. Assuming ρ small such that $\frac{\rho \mathcal{L}}{2} \sum \|\nabla\|^2 \leq \frac{\eta}{4\epsilon} \sum \|\nabla\|^2$ (absorbed by choice), divide by T :

$$\frac{1}{T} \sum_{t=1}^T \|\nabla L(\theta_t)\|^2 \leq \frac{2\epsilon(L(\theta_1) - L^*)}{\eta T} + 2\rho\mathcal{L} + O(\epsilon^2 d\mathcal{L}) + O\left(\frac{\mathcal{L}\eta}{\epsilon T}(L(\theta_1) - L^*)\right) \quad (92)$$

$$+ O\left(\frac{\epsilon}{\eta} \sqrt{\frac{\mathcal{L}d(\sigma^2 + \epsilon^2 G^2)(L(\theta_1) - L^*)}{mT}}\right). \quad (93)$$

To balance terms, set $\eta = O\left(\sqrt{\frac{\epsilon^2(L(\theta_1) - L^*)}{\mathcal{L}T}}\right)$:

$$\frac{1}{T} \sum_{t=1}^T \mathbb{E}\|\nabla L(\theta_t)\|^2 \leq O\left(\sqrt{\frac{\mathcal{L}(L(\theta_1) - L^*)}{T}}\right) + 2\rho\mathcal{L} \quad (94)$$

$$+ \sqrt{\frac{4d\mathcal{L}(L(\theta_1) - L^*)(\sigma^2 + \epsilon^2 G^2)}{mT}} + O(\epsilon^2 d\mathcal{L}). \quad (95)$$

For flat minima bias: ZO introduces Hessian trace bias $O(\epsilon\sqrt{d} \text{Tr}(H))$ in gradient estimates, enhanced by SAM's ρ -regularization approximating $\min L + \rho\|\nabla\|$, leading to stationary points with $\mathbb{E}[\text{Tr}(H(\bar{\theta}))] \leq \min \text{Tr}(H^*) + O(\rho + \epsilon\sqrt{d})$.

B.2 PROOF OF THEOREM 4.4

We employ the PAC-Bayesian framework to bound the generalization error. The PAC-Bayesian theorem states that, for any prior distribution p and posterior distribution q (possibly dependent on \mathcal{S}), with probability at least $1 - \kappa$ over the draw of \mathcal{S} :

$$\mathbb{E}_{q(x)} [\mathbb{E}_{P(X,y)}[F(x; (X, y))]] \leq \mathbb{E}_{q(x)}[F(x; \mathcal{S})] + \sqrt{\frac{\text{KL}(q \parallel p) + \log\left(\frac{M}{\kappa}\right)}{M - 1}}. \quad (96)$$

We set the posterior $q = \mathcal{N}(\theta_t, \epsilon I)$ for small $\epsilon > 0$, approximating the deterministic parameter θ_t at iteration t .

To handle the adaptive neighborhood, we define an effective radius $r_t = \rho/\sigma_t$, where σ_t is the adaptive standard deviation computed in ZOSA. We select a prior $p = \mathcal{N}(0, \sigma_p^2 I)$ from a discretized set $\mathcal{T} = \{c \exp(j/k) \mid j \in \mathbb{Z}\}$ for some constant $c > 0$, ensuring coverage of possible σ_p^2 values close to $r_t^2/(1 + \sqrt{\log M/k})^2$.

Substituting into the PAC-Bayesian bound and applying a union bound over $|\mathcal{T}|$ priors (with $|\mathcal{T}| \approx \log M$ for appropriate discretization), we have, with probability at least $1 - \kappa$:

$$\mathbb{E}_{x \sim q} [\mathbb{E}_{P(X,y)}[F(x; (X, y))]] \leq \mathbb{E}_{x \sim q}[F(x; \mathcal{S})] \quad (97)$$

$$+ \sqrt{\frac{\text{KL}(q \parallel p) + \log\left(\frac{M|\mathcal{T}|}{\kappa}\right) + \tilde{O}(1)}{M - 1}}, \quad (98)$$

for the optimal $p \in \mathcal{T}$.

The KL divergence for Gaussian q and p is:

$$\text{KL}(q \parallel p) = \frac{1}{2} \left[k \log \frac{\sigma_p^2}{\epsilon^2} + k \left(\frac{\epsilon^2}{\sigma_p^2} - 1 \right) + \frac{\|\theta_t\|_2^2}{\sigma_p^2} \right]. \quad (99)$$

By choosing $\sigma_p^2 \approx r_t^2/(1 + \sqrt{\log M/k})^2$ and taking $\epsilon \rightarrow 0$ (with appropriate bounding), the dominant term simplifies to:

$$\text{KL}(q \parallel p) \leq k \log \left(1 + \frac{\|\theta_t\|_2^2}{r_t^2 \left(1 + \sqrt{\frac{\log M}{k}} \right)^2} \right) + \tilde{O}(1). \quad (100)$$

Incorporating the union bound, $\log(|\mathcal{T}|M/\kappa) \leq 4\log(M/\kappa) + \tilde{O}(1)$ for suitable discretization.

The sharpness-aware objective in ZOSA minimizes the maximum loss in the adaptive L_2 neighborhood:

$$\max_{\|\delta\|_2 \leq r_t} F(\theta_t + \delta; \mathcal{S}). \quad (101)$$

Since $\mathbb{E}_{x \sim q}[F(x; \mathcal{S})] \leq \max_{\|\delta\|_2 \leq r_t} F(\theta_t + \delta; \mathcal{S})$ (as q concentrates around θ_t and the neighborhood captures perturbations up to r_t via concentration inequalities for Gaussian perturbations approximating the L_2 ball),

we refine the bound:

$$\mathbb{E}_{x \sim q} [\mathbb{E}_{P(X,y)}[F(x; (X, y))]] \leq \max_{\|\delta\|_2 \leq r_t} F(\theta_t + \delta; \mathcal{S}) \quad (102)$$

$$+ \sqrt{\frac{k \log \left(1 + \frac{\|\theta_t\|_2^2}{r_t^2 \left(1 + \sqrt{\frac{\log M}{k}} \right)^2} \right) + 4 \log \frac{M}{\kappa} + \tilde{O}(1)}{M - 1}}. \quad (103)$$

Assuming the loss function $F(x; (X, y))$ is convex with respect to x , Jensen's inequality applies in the limit $\epsilon \rightarrow 0$:

$$\mathbb{E}_{P(X,y)}[F(\theta_t; (X, y))] = \mathbb{E}_{P(X,y)}[F(\mathbb{E}_{x \sim q}[x]; (X, y))] \quad (104)$$

$$\leq \mathbb{E}_{x \sim q} [\mathbb{E}_{P(X,y)}[F(x; (X, y))]]. \quad (105)$$

Combining this with the previous bound yields the final result:

$$\mathbb{E}_{P(X,y)}[F(\theta_t; (X, y))] \leq \max_{\|\delta\|_2 \leq \rho/\sigma_t} F(\theta_t + \delta; \mathcal{S}) \quad (106)$$

$$+ \sqrt{\frac{k \log \left(1 + \frac{\|\theta_t\|_2^2}{(\rho/\sigma_t)^2 \left(1 + \sqrt{\frac{\log M}{k}} \right)^2} \right) + 4 \log \frac{M}{\kappa} + \tilde{O}(1)}{M - 1}}. \quad (107)$$

C ADDITIONAL MATERIAL FOR SECTION 5

C.1 ADDITIONAL DETAILS ON SYNTHETIC FUNCTIONS EXPERIMENTS

Function Definitions: Let input $\theta = [\theta]_{i=1}^d$, the Quadratic, Cubic, Levy, and Rosenbrock functions applied in our synthetic experiments are given below:

$$F(\theta) = \frac{1}{2} \sum_{i=1}^d \theta_i^2, \quad (108)$$

$$F(\theta) = \sum_{i=1}^d |\theta_i|^3 + \frac{\theta_i^2}{2}, \quad (109)$$

$$F(\theta) = \sin^2(\pi w_1) + \sum_{i=2}^{d-1} (w_i - 1)^2 [1 + 10 \sin^2(\pi w_{i+1})] + (w_d - 1)^2 [1 + \sin^2(2\pi w_d)], \quad (110)$$

$$F(\theta) = \sum_{i=1}^{d-1} [100(\theta_{i+1} - \theta_i^2)^2 + (1 - \theta_i)^2], \quad (111)$$

where $w_i = 1 + \frac{\theta_i - 1}{4}$. Note that all functions have the same minimum of zero, i.e., $\min F(\theta) = 0$.

Experimental Setup for Additional Dimensions: To comprehensively evaluate the effectiveness of the zeroth-order (ZO) optimizer across varying problem dimensions, we extended our experimental analysis to include settings with $d = 1000$ and $d = 5000$, in addition to $d = 10000$. This expansion

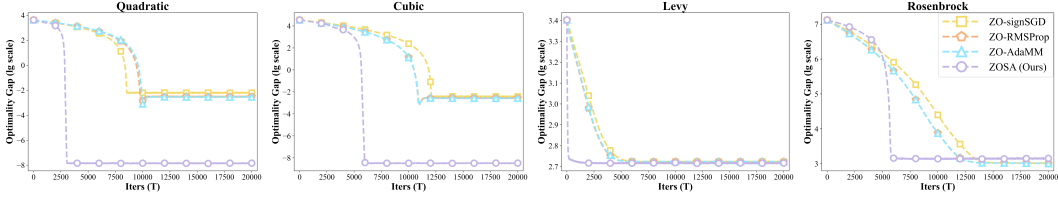


Figure 4: Results on the four test functions with problem dimension $d = 1000$ and $K = 100$.

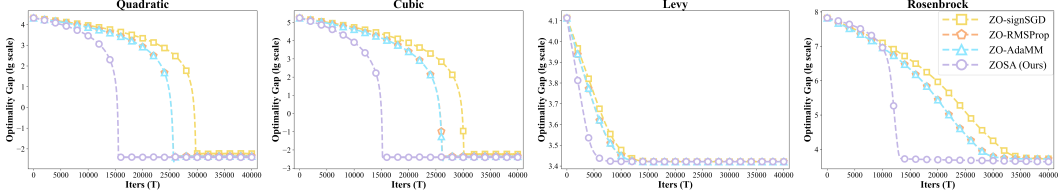


Figure 5: Results on the four test functions with problem dimension $d = 5000$ and $K = 500$.

allows us to assess the scalability and robustness of ZOSA under more challenging conditions. For all optimizers, including ZOSA and established baselines, we performed a hyperparameter search for learning rates within the range $[1e - 5, 1e - 2]$, ensuring a fair comparison between different dimensionalities and optimization landscapes.

To further tailor the experimental setup to the unique characteristics of ZOSA, we adjusted the number of perturbation vectors K (equivalent to m in ZOSA) and the smoothing parameter μ based on the problem dimension. Specifically, we set $K = 100$, $K = 500$, and $K = 1000$ for $d = 1000$, $d = 5000$, and $d = 10000$ respectively, with $\mu = 0.005$ across all cases. Additionally, for ZOSA, we performed a specialized hyperparameter search for its parameter ρ (controlling the sharpness-aware perturbation scale) within the range $[1e - 7, 1e - 3]$. This adaptive tuning of ρ allows ZOSA to dynamically adjust its perturbation magnitude, leveraging its variance-aware mechanism to enhance gradient estimation accuracy in high-dimensional spaces.

Fig. 4 and Fig. 5 present the detailed comparison of the performance of all optimizers across these dimensions, highlighting convergence rates and stability. Fig. 6 and Fig. 7 illustrate the cosine similarity between the true gradient and the estimated gradient, a critical metric for evaluating the quality of ZO gradient approximations. The results demonstrate that ZOSA consistently achieves higher cosine similarity values, particularly in high-dimensional and non-convex settings, owing to its innovative use of variance-reduced first moment estimates and refined second moment scaling. This superior alignment with true gradients underscores ZOSA’s advantage in delivering stable and accurate gradient estimates, even as dimensionality increases. Furthermore, the adaptive learning rate adjustment based on $\sigma_{t_{pert}}$ enables ZOSA to outperform baselines by effectively navigating complex optimization landscapes, making it a robust choice for real-world applications.

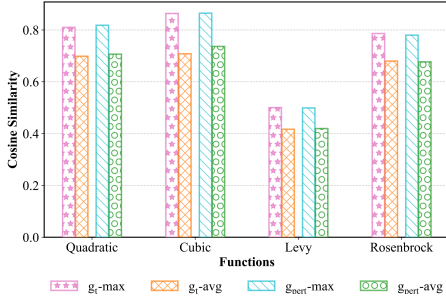


Figure 6: Cosine similarity between the estimated gradients and the true gradients with problem dimension $d = 1000$.

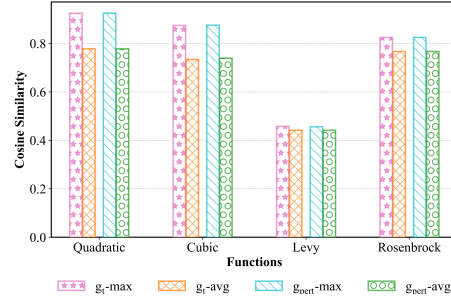


Figure 7: Cosine similarity between the estimated gradients and the true gradients with problem dimension $d = 5000$.

C.2 ADDITIONAL DETAILS ON ZERO-ORDER PROMPT FINE-TUNING

Fig. 8 and Fig. 9 showcase the comparison of ZOSA and SABO accuracy and query times across six NLP benchmarks at intrinsic dimensions $d = 200$ and $d = 500$, respectively. ZOSA highlights its advantage with adaptive efficiency, achieving competitive accuracy with lower query times, excelling in higher-dimensional scalability. These results underscore ZOSA’s adaptability and cost-effectiveness in lower dimensions.

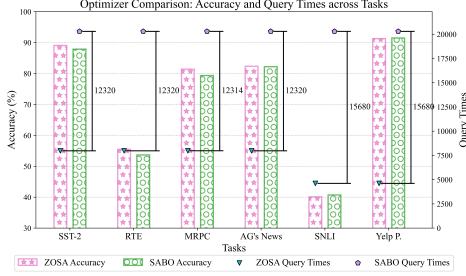


Figure 8: Comparison of ZOSA and SABO optimizers in terms of accuracy (%) and query times across six prompt learning tasks with $d = 200$.

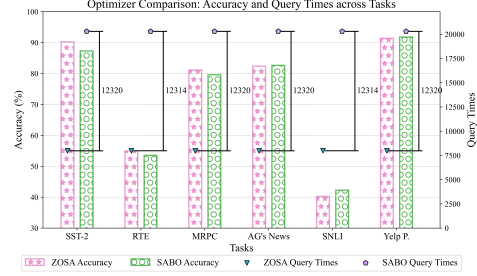


Figure 9: Comparison of ZOSA and SABO optimizers in terms of accuracy (%) and query times across six prompt learning tasks with $d = 500$.

Implementation Details. We employ a fixed, randomly initialized projection matrix $A \in \mathbb{R}^{d \times D}$ to map a vector $v \in \mathbb{R}^d$ into the token embedding space \mathbb{R}^D . Consequently, we focus on optimizing $v \in \mathbb{R}^d$ rather than the prompt $p \in \mathbb{R}^D$ directly. The pre-trained RoBERTa-large model (Liu et al., 2019) serves as the foundational architecture, with the matrix A sampled from a normal distribution as outlined in (Sun et al., 2023), specifically $\mathcal{N}(0, \sigma_e \sqrt{d})$, where σ_e represents the standard deviation of word embeddings in RoBERTa-large. For ZOSA, along with comparative methods including CMA-ES (Hansen, 2006), MMES (He et al., 2020), BES (Gao & Sener, 2022), INGO (Lyu & Tsang, 2022), and SABO (Ye et al., 2024), the cross-entropy loss on the training data serves as the zero-order optimization objective across six datasets, with optimization of v conducted subject to a budget of 8,000 evaluations. Initial Gaussian distributions are set with mean $\mu_0 = 0$ and covariance $\Sigma_0 = I$, with a perturbation population size m for ZOSA searched over $\{4, 8, 16\}$ and $N = 100$ for all other optimizers. Hyperparameter tuning via grid search is applied to ZOSA, INGO, BES, and SABO, with the learning rate η for ZOSA explored over $\{1e-6, 1e-5, 1e-4\}$, the sharpness-aware neighborhood size ρ over $\{1e-6, 1e-5, 1e-4, 1e-3, 1e-2\}$ for ZOSA and over $\{10, 50, 100, 500\}$ for SABO, the learning rate β for INGO, BES, and SABO over $\{0.1, 0.5, 1, 5\}$, and the spacing parameter c for BES over $\{0.1, 1, 10\}$. Additionally, we evaluate all methods across varying dimensions of v , specifically $d \in \{200, 500, 1000\}$. Each experiment is replicated three times independently, reporting mean objective values with standard deviations.